



A General Load–Displacement Relationship Between Random Rough Surfaces in Elastic, Non-adhesive Contact, with Application in Metal Additive Manufacturing

J. Joe¹ · J. R. Barber² · B. Raeymaekers¹

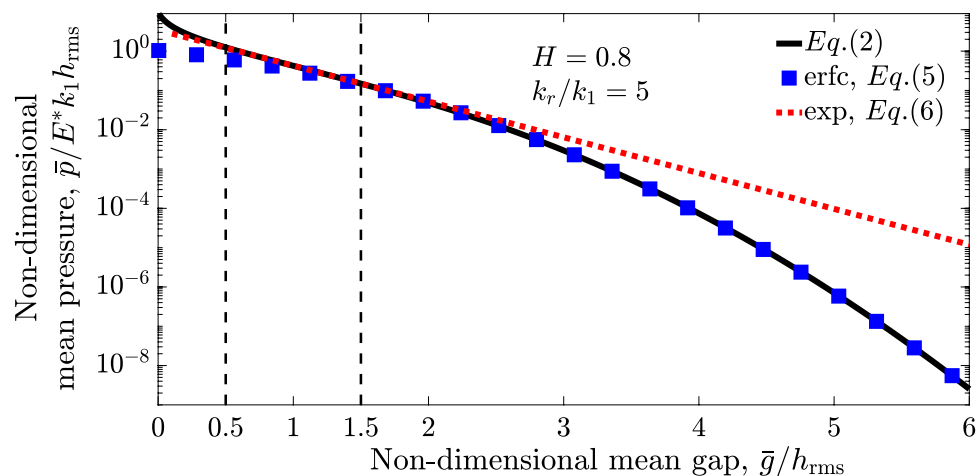
Received: 18 March 2022 / Accepted: 16 May 2022

© The Author(s), under exclusive licence to Springer Science+Business Media, LLC, part of Springer Nature 2022

Abstract

The load–displacement relationship between two rough surfaces in contact determines physical properties such as thermal and electrical conductivity, contact stiffness, and leakage rate. Thus, many researchers have studied the relationship between the mean pressure and the mean gap of isotropic, Gaussian, random rough surfaces in contact, using theoretical and numerical multi-asperity models, and using fractal models that account for multi-scale roughness. However, fractal models are sometimes difficult to use in practice because they require numerical solution. Hence, in this paper, we provide best-fit regression equations that approach the numerical solutions of fractal models to enable straightforward use in engineering applications. We show that the load–displacement relationship between random rough surfaces is best approximated by an exponential function and by a complementary error function depending on the magnitude of the gap between the surfaces. We illustrate the application of the best-fit regression equations for contact of an as-built Inconel 718 surface manufactured with laser powder bed fusion. This work enables applying complex contact models to engineering problems in a straightforward fashion.

Graphical Abstract



Keywords Contact mechanics · Surface topography · Traction · Surface separation · Additive manufacturing

✉ B. Raeymaekers
bart.raeymaekers@utah.edu

¹ Department of Mechanical Engineering, University of Utah, Salt Lake City, UT 84112, USA

² Department of Mechanical Engineering, University of Michigan, Ann Arbor, MI 48109, USA

1 Introduction

It is well-known that unlubricated contact between two rough surfaces occurs at the peaks or asperities of the surface roughness [1]. Hence, the surface roughness determines

the load–displacement relationship between contacting rough surfaces, which plays an important role in estimating electrical and thermal conductivity [2], the leakage rate between contacting surfaces in seals [3, 4], and incremental contact stiffness [5] to predict, e.g., the dynamic response of structures with bolted joints [6]. The load–displacement or so-called “traction” relationship is expressed as the mean contact pressure \bar{p} , which is the normal load divided by the nominal contact area, as a function of the mean gap \bar{g} , which is the distance between the mean lines of the roughness profiles of both contacting surfaces [7].

Determining the load–displacement relationship of contacting rough surfaces using numerical simulations is computationally expensive because a fine mesh is required to accurately capture surface roughness features [8, 9]. Thus, theoretical models, which provide closed-form rather than numerical solutions, are useful to establish a fundamental understanding of the effect of surface roughness on the traction relationship of contacting rough surfaces. Greenwood and Williamson, GW [10] first documented a statistical multi-asperity contact model that represents surface roughness as multiple, identical, spherical asperities with a Gaussian or exponential distribution of asperity heights. Later, Bush et al., BGT [11] extended the GW model to include spherical asperities with different radii, determined from Nayak’s random process theory [12].

However, asperity models and their extensions do not account for interactions between individual asperities and do not easily accommodate multi-scale surface roughness [13]. In contrast, multi-scale contact models characterize the surface roughness using the power spectral density (PSD) $P(k)$ [14], with k the wavenumber, i.e.,

$$P(k) = \begin{cases} C_0, & k_1 \leq k \leq k_r, \\ C_0(k/k_r)^{-2(H+1)}, & k_r < k \leq k_2, \\ 0, & k > k_2, \end{cases} \quad (1)$$

where k_1 , k_r , and k_2 are the lower, roll-off, and upper wavenumber, H is the Hurst exponent, and C_0 is a scaling constant. Within the fractal range $k_r < k \leq k_2$, the surface roughness exhibits self-affinity and the PSD follows a power law with $0 < H < 1$ or a fractal dimension $D \equiv 3 - H$. Most engineering surfaces display $H > 0.5$ [15]. Outside the fractal range $k < k_r$, the PSD is approximately constant [16].

Theoretical contact models that implement multi-scale surface roughness resolve some of the intrinsic shortcomings of asperity models. Ciavarella et al. [17] studied contact between an elastic half-plane and a rigid multi-scale rough surface defined by a Weierstrass series that represents an idealized PSD with a discrete set of wavenumbers, and they used recursive integration to show that the real contact area decreases when increasing the upper limit of

the wavenumber in the Weierstrass series. Persson [18] considered elastic contact of random rough surfaces with a continuous PSD, and determined the effect of including progressively finer roughness scales on the probability that contact occurs for any contact pressure. He assumed that the additionally introduced roughness remains in full contact, which required introducing a semi-empirical correction factor to account for overestimating the stored elastic energy [19, 20].

Joe et al. [21] implemented a theoretical model to predict the traction relationship for elastic contact between isotropic, Gaussian, and random rough surfaces, without requiring a semi-empirical correction factor. This model is described in detail in reference [22] and shows good agreement with direct numerical simulations, including the boundary element method, BEM [23] and Green’s function molecular dynamics, GFMD [9]. However, the formulation of this model requires a numerical solution of the traction relationship, which prevents easy use in engineering applications.

Hence, in this paper, we attempt to overcome this difficulty by numerically solving the theoretical model of Joe et al. [21], and deriving best-fit regression equations that describe the traction relationship between realistic engineering surfaces in non-adhesive, unlubricated, elastic contact. We show that the best-fit regression equations follow an exponential or complementary error function depending on the magnitude of the mean gap \bar{g} , and we observe that the regression coefficients are a function of H and k_r/k_1 . Finally, we use the best-fit regression equations to determine the traction relationship for contact between as-built metal additive manufactured surfaces, as an illustrative case study.

2 Theoretical Model

We idealize the random rough surfaces as a superposition of random roughness of multiple spatial frequencies. Figure 1a shows a continuous PSD of a rough surface with $k_1 \leq k \leq k_2$, which decomposes into coarse-scale ($k_1 \leq k \leq k^*$) and fine-scale ($k^* \leq k \leq k_2$) roughness. Figure 1b schematically illustrates elastic contact between two random rough surfaces as contact between an equivalent rough surface that contains the coarse-scale roughness and a rigid flat [24], and the local traction relationship $p(g; k^*, k_2)$ implicitly includes the effect of the fine-scale roughness ($k^* \leq k \leq k_2$). The Young’s modulus of the equivalent rough surface $E^* = ((1 - \nu_1^2)/E_1 + (1 - \nu_2^2)/E_2)^{-1}$, with E_1 , E_2 , ν_1 , and ν_2 the Young’s modulus and Poisson coefficient of both contacting random rough surfaces, respectively. Figure 1b also shows the local gap g , mean gap \bar{g} , and local surface height $h = g - \bar{g}$ measured from the mean line of the equivalent roughness profile.

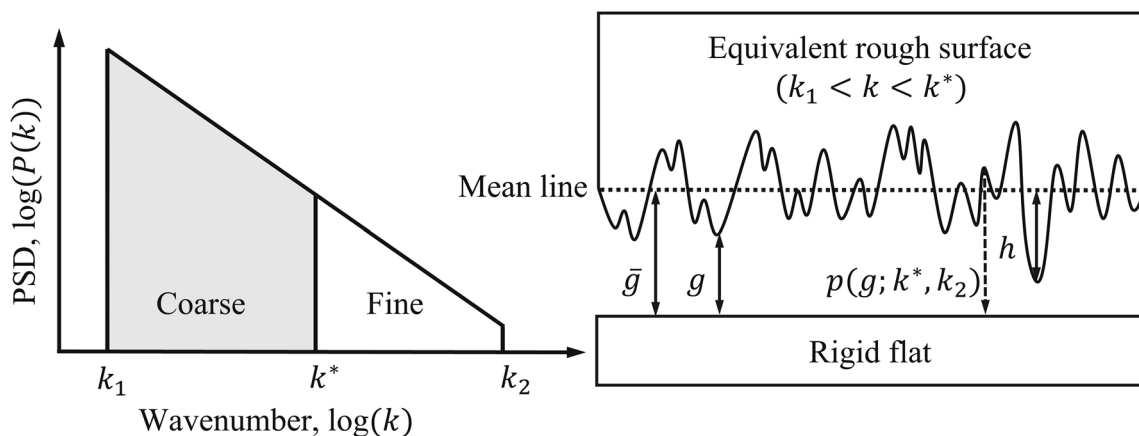


Fig. 1 **a** Schematic illustration of the power spectral density of a random rough surface, indicating coarse ($k_1 \leq k \leq k^*$) and fine-scale ($k^* \leq k \leq k_2$) roughness. **b** Schematic of an equivalent rough surface containing coarse-scale roughness in contact with a rigid flat, show-

ing the mean gap \bar{g} , local gap g , surface height $h \equiv \bar{g} - g$, and local traction relationship $p(g; k^*, k_2)$ that implicitly includes the effect of fine-scale roughness

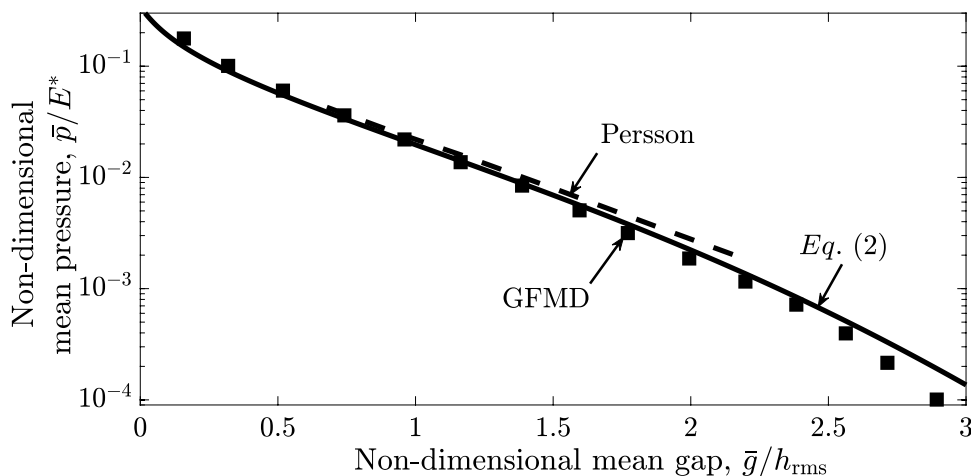
We succinctly review the key aspects of the theoretical model [21, 22]. It is challenging to sum the effect of random roughness of multiple scales on the traction relationship because even a smooth elastic problem requires solving a second order partial differential equation with fourth rank tensors. The theoretical model [21, 22] simplifies this problem as follows. When we only consider coarse-scale roughness $k_1 \leq k \leq k^*$, instead of considering the entire spectrum of roughness scales $k_1 \leq k \leq k_2$, we modify contact between the rough surfaces by neglecting the fine-scale roughness $k^* < k < k_2$, and we obtain an “effective” traction relationship, $p(g; k^*, k_2)$. This effective traction relationship derives from the product between the probability density function of the gap g between the fine-scale roughness $k^* < k < k_2$ and a rigid flat $\Phi(g|\bar{g}; k^*, k_2)$. When k^* approaches k_1 , we obtain the traction relationship that considers the entire roughness $\bar{p}(\bar{g})$. Thus, the theoretical model [21, 22] explicitly considers the coarse-scale roughness, whereas it includes

the fine-scale roughness implicitly in the effective traction relationship.

The traction relationship that considers the entire roughness spectrum $k_1 \leq k \leq k_2$ results from including gradually coarser roughness, i.e., k^* approaches k_1 (see Fig. 1a), and requires using a recursive solution procedure [21], similar to other theoretical models [17, 18]. We previously converted this recursive method to a partial differential equation to reduce computational complexity [22], i.e.,

$$\frac{\partial p}{\partial k}(g; k, k_2) = \frac{1}{2} \left[2\pi k P(k) \left(1 - \frac{2}{E^* k} \frac{\partial p(g; k, k_2)}{\partial g} \right)^{-2} \right] \frac{\partial^2 p}{\partial g^2}(g; k, k_2). \quad (2)$$

Fig. 2 The non-dimensional mean pressure \bar{p}/E^* as a function of the non-dimensional mean gap \bar{g}/h_{rms} , for Eq. (2) (solid line), GFMD (square markers) and Persson (dashed line) models, using the rough surface from the “contact mechanics challenge” [9]



2.1 Comparison with Numerical Computation

Figure 2 shows a comparison of the traction relationship, i.e., the non-dimensional mean pressure \bar{p}/E^* as a function of the non-dimensional mean gap \bar{g}/h_{rms} , for the theoretical models of Eq. (2) [22] (solid line) and Persson [16] (dashed line), and the GFMD [25] (square markers) numerical simulation, using the rough surface defined in the “contact mechanics challenge” [9]. The results of the “contact mechanics challenge” [9] show that the direct numerical simulations agree very well, while among the theoretical predictions (including asperity-based models), Persson’s model showed the best agreement with the numerical result. Both theoretical models show good agreement with the numerical simulation for $\bar{g}/h_{rms} \leq 2$, but they diverge with increasing mean gap because of the so-called finite height effect [26]. Theoretical models consider an ideal rough surface with Gaussian distribution of surface heights, which results in contact for any mean gap \bar{g}/h_{rms} . In contrast, numerical approximations of a random rough surface inevitably require a finite maximum surface height, which limits contact to finite values of the mean gap \bar{g}/h_{rms} and, therefore, underestimates the mean contact pressure \bar{p}/E^* for $\bar{g}/h_{rms} > 2$.

2.2 Dimensional Analysis

Persson [27] and Pohrt and Popov [28] non-dimensionalized the traction relationship for non-adhesive, elastic contact of random rough surfaces as

$$\frac{\bar{p}(\bar{g})}{E^* h_{rms} k_1} = f\left(\frac{\bar{g}}{h_{rms}}\right). \tag{3}$$

Substituting Eq. (3) in Eq. (2), re-formulates the differential equation in terms of the PSD, $P(k)$, which depends on the Hurst exponent H , the ratio of roll-off and lower wavenumber k_r/k_1 , and the ratio of upper and lower wavenumber

k_2/k_1 . Engineering surfaces typically show $H > 0.5$, and the traction relationship converges with sufficiently large k_2/k_1 [27, 29], because the average roughness beyond k_2 approaches zero. As such, the function f only depends on the PSD shape factors H and k_r/k_1 . It asymptotically approaches the vertical when $\bar{g} \rightarrow 0$ and shows a concave downward trend with increasing \bar{g} .

2.2.1 Complementary Error Function Approximation

Numerical [30, 31], theoretical [10, 11, 18], and experimental [32, 33] studies demonstrated that the mean contact pressure is approximately proportional to the ratio of the real and nominal contact area $A_{real}/A_{nominal}$ for $A_{real}/A_{nominal} < 0.15$, i.e.,

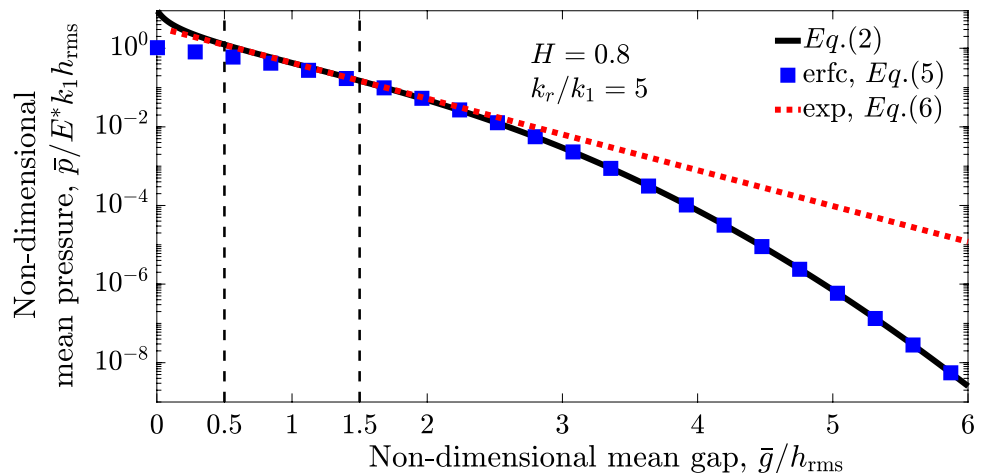
$$\frac{A_{real}}{A_{nominal}} \propto \frac{\bar{p}}{E^*}. \tag{4}$$

Additionally, asperity models [11, 34] approximate the real contact area for a small normal load by calculating half of the area underneath the probability density function of the local gap between the equivalent rough surface and the rigid flat, $\Phi(g)$, for $g \leq \bar{g}$. Hence, we approximate the non-dimensional traction relationship equation (3) as

$$\frac{\bar{p}(\bar{g})}{E^* h_{rms} k_1} = A \operatorname{erfc}\left(\frac{\bar{g}}{B h_{rms}}\right). \tag{5}$$

The BGT model [11] determined that parameter $B = \sqrt{2}$ in Eq. 5, based on the assumption that the asperities do not interact with each other. In contrast, in this work, we maintain parameter B as a regression parameter, because the mean gap decreases with increasing contact pressure and, thus, asperities can interact with each other.

Fig. 3 The non-dimensional mean pressure $\bar{p}/E^* k_1 h_{rms}$ as a function of the non-dimensional mean gap \bar{g}/h_{rms} for a random rough surface with $H = 0.8$ and $k_r/k_1 = 5$, showing the solution of Eq. (2) (solid line), and best-fit results for the complementary error function [square markers, see Eq. (5)] and exponential function [dotted line, see Eq. (6)]



2.2.2 Exponential Approximation

When applying a large normal load to the contacting rough surfaces, the mean gap is small and the real contact area is large. Thus, increasing the mean pressure increases the number of asperities that make contact. However, the probability density function of both the size of the contact points and the local contact pressure remain almost constant, independent of the number of asperities that make contact [35, 36]. Hence, the stored elastic energy is proportional to the mean contact pressure [26], which in turn explains the linear relationship between the mean contact pressure and the incremental stiffness, i.e., $\bar{p} \propto \partial \bar{p} / \partial \bar{g}$, which is in agreement with experimental observations [37]. Here, an exponential function accommodates the linear relationship between the mean contact pressure and the incremental stiffness. Hence, we approximate the non-dimensional traction relationship as [38]

$$\frac{\bar{p}(\bar{g})}{E^* h_{rms} k_1} = A \exp\left(-\frac{\bar{g}}{B h_{rms}}\right). \tag{6}$$

Persson [27] determined that parameter $B = \gamma/\alpha$ in Eq. 6, with $\gamma \approx 0.48$ and $\alpha \approx 1$, for $H=0.8$. In contrast, in this work, we determine parameters A and B in Eqs. (5) and (6) using regression analysis, as a function of the two shape factors of the PSD, H and k_r/k_1 . We show that Eqs. (5) and (6) establish a best-fit for the traction relationship of non-adhesive, elastic contact between isotropic, Gaussian, and random rough surfaces for a large and small non-dimensional mean gap, respectively.

3 Results and Discussion

Figure 3 shows the non-dimensional mean pressure $\bar{p}/E^* k_1 h_{rms}$ as a function of the non-dimensional mean gap \bar{g}/h_{rms} for a random rough surface with $H = 0.8$ and $k_r/k_1 = 5$, derived using Eq. (2) (solid line). We superimpose the best-fit regression results using the complementary error function [square markers, see Eq. (5)] and exponential function [dotted line, see Eq. (6)].

From Fig. 3 we observe that the exponential function provides the best-fit with the theoretical model when $0.5 \leq g/h_{rms} \leq 1.5$ with parameters $A = 3.463$ and $B = 0.4769$. Figure 3 also shows that the complementary error function provides the best-fit when $1.5 \leq g/h_{rms} \leq 6.0$ with parameters $A = 1.038$ and $B = 1.424 (\approx \sqrt{2})$, with $R^2 = 1.000$, as expected from asperity models. This also explains results presented by Buzio et al. [39], who used a flat punch experiment to show that the traction relationship deviates from the exponential function with increasing mean gap (or decreasing mean pressure).

Overall, the results in Fig. 3 are in agreement with the observations documented by Papangelo et al. [40], who concluded that the exponential approximation of Eq. (6) matches direct numerical simulations using, e.g., the BEM for an “intermediate range” ($0.5 \leq \bar{g}/h_{rms} \leq 1.5$), whereas the complementary error function approximation of Eq. (5) improves with increasing mean gap ($\bar{g}/h_{rms} > 1.5$) for $H = 0.8$ and $k_r/k_1 = 1$. The regression parameters A and B in Eqs. (5) and (6) that yield the best-fit of Eq. (2) depend only on the shape factors of the PSD of the equivalent roughness, i.e., H and k_r/k_1 .

Figure 4a shows the parameters A and B of the complementary error function of Eq. (5) as a function of H for $k_r/k_1 = 1$ and with $1.5 \leq g/h_{rms} \leq 6.0$. Parameter A decreases whereas parameter $B = \sqrt{2}$ remains almost

Fig. 4 Parameters A and B in the complementary error best-fit function [see Eq. (5)] with $1.5 \leq g/h_{rms} \leq 6.0$, **a** as a function of the Hurst exponent H with $k_r/k_1 = 1$ and **b** parameter A (solid line) and $A/(k_r/k_1)$ (dotted line) as a function of k_r/k_1 for different values of H (B is constant with respect to k_r/k_1)

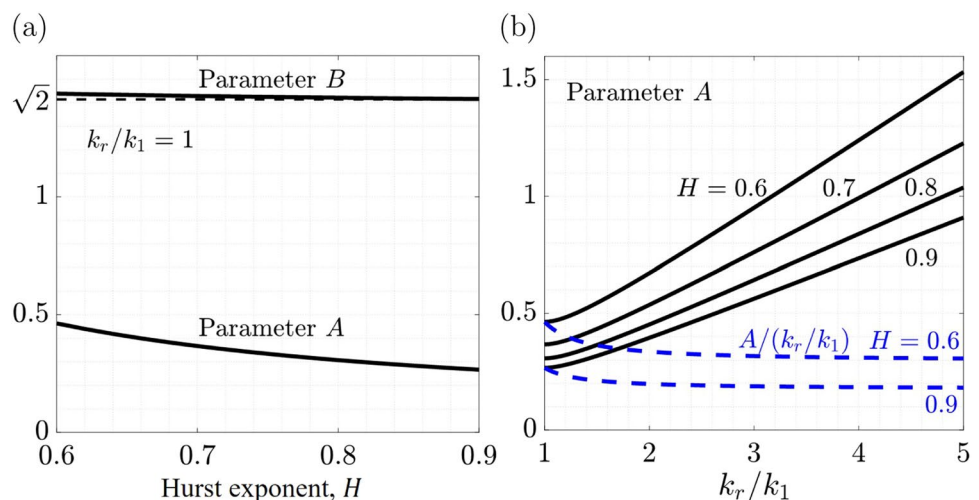
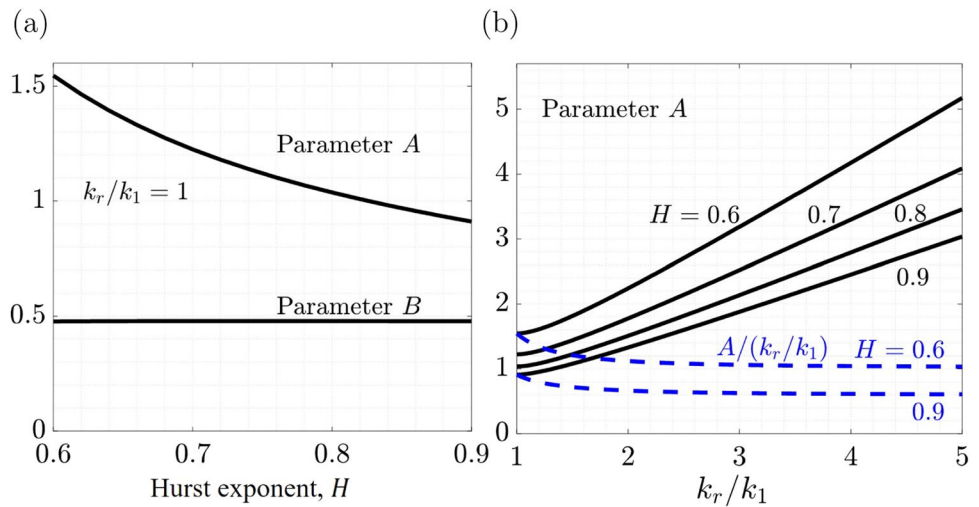


Fig. 5 Parameters *A* and *B* in the exponential best-fit function [see Eq. (6)] with $0.5 \leq g/h_{rms} \leq 1.5$, **a** as a function of the Hurst exponent *H* with $k_r/k_1 = 1$ and **b** parameter *A* (solid line) and $A/(k_r/k_1)$ (dotted line) as a function of k_r/k_1 for different values of *H* (*B* is constant with respect to *H* and k_r/k_1)



constant with increasing *H*. Furthermore, we determine that parameter *B* is also independent of k_r/k_1 . Figure 4b shows parameter *A* as a function of k_r/k_1 for different values of *H* (solid line). We observe that parameter *A* increases with increasing k_r/k_1 and decreasing *H*. Increasing k_r/k_1 and decreasing *H* increases the contribution of fine-scale roughness for constant h_{rms} and k_1 , which, in turn, increases the mean pressure. Parameter *A* shows a linear trend for $k_r/k_1 > 1.4$ and, thus, we also display $A/(k_r/k_1)$ (dotted line), which approaches an asymptote with increasing k_r/k_1 depending on *H*. Increasing k_r/k_1 with constant scaling factor C_0 [see Eq. (1)] does not significantly affect h_{rms} , which renders parameter *A* primarily dependent on k_r/k_1 .

Based on the results of Fig. 4, we write parameters *A* and *B* as,

$$A(H, k_r/k_1) = (0.2565H^{-2.211} + 0.3505)(k_r/k_1) \times \frac{0.2652(k_r/k_1)^3 + 0.1737(k_r/k_1)^2 - 0.3002(k_r/k_1) + 0.05017}{(k_r/k_1)^3 + 0.7047(k_r/k_1)^2 - 1.852(k_r/k_1) + 0.6203}, \quad (7)$$

$$B(H) = -0.1333H^3 + 0.3848H^2 + -0.4238H + 1.582. \quad (8)$$

The maximum error between the best-fit equation (7) and the results of Fig. 4 is approximately 1.3%, when $H = 0.6$ and $k_r/k_1 = 1$.

Figure 5a shows the parameters *A* and *B* of the exponential best-fit function of Eq. (6) as a function of *H* for $k_r/k_1 = 1$ and with $0.5 \leq g/h_{rms} \leq 1.5$. We observe a similar trend as for the complementary error function in Fig. 4. Parameter *A* decreases whereas parameter *B* remains almost constant with increasing *H*. Furthermore, parameter $B = 0.478$ is also independent of k_r/k_1 . This result is in agreement with earlier research [5, 40], which showed that parameter $B \approx 0.48$ and independent of *H* in the exponential approximation.

Figure 5b shows parameter *A* (solid line) and $A/(k_r/k_1)$ (dotted line) as a function of k_r/k_1 for different values of *H*, revealing a similar trend as in Fig. 4b. We note that the ratio of parameter *A* in the complementary error function and exponential function approximation is 0.3 with a

Fig. 6 Inconel 718 specimen manufactured with L-PBF, showing **a** schematic and picture of a dogbone specimen and **b** confocal microscopy image of the surface topography of the as-built surface

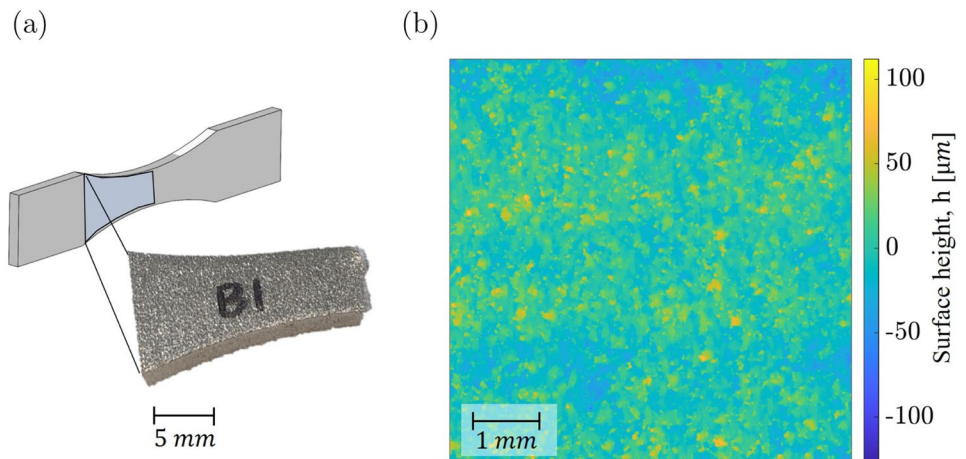
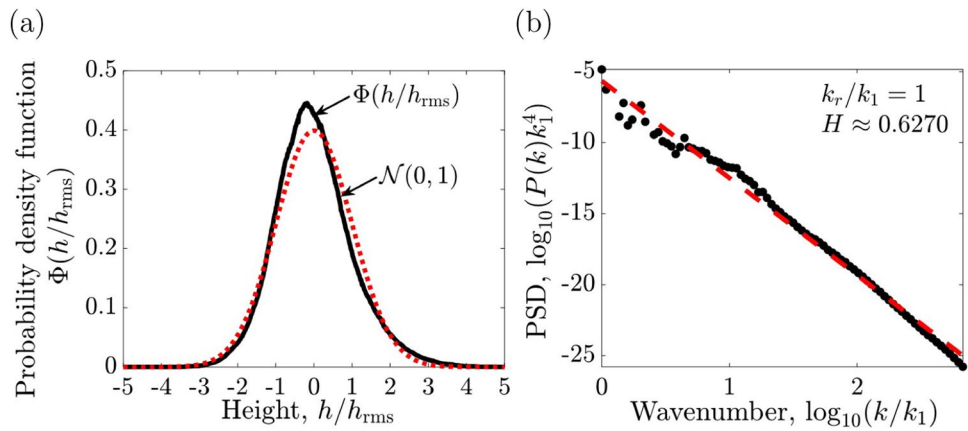


Fig. 7 **a** The probability density function of the dimensionless surface height (h/h_{rms}) (solid line) compared to the standard normal distribution $\mathcal{N}(0, 1)$ (dotted line), and **b** the PSD of the surface topography of the specimen (circle markers) and its linear curve fit (dashed line)



maximum error of 3% compared to the value of parameter A obtained from the regression analysis with exponential function.

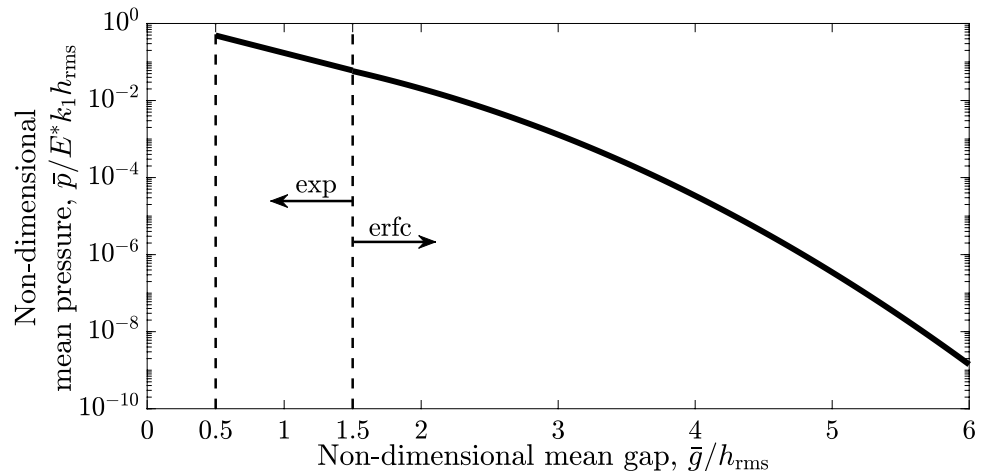
4 Case Study: Contact Between As-built Inconel 718 Surfaces Manufactured with Laser Powder Bed Fusion (L-PBF)

We use the best-fit regression equations we have derived from the theoretical model to calculate and understand the traction relationship of an as-built Inconel 718 surface manufactured with L-PBF in contact with a rigid flat, as an illustrative case study. Inconel 718 is used in aerospace and nuclear applications because its strength at elevated temperature and its corrosion resistance [41]. However, the surface topography of the as-built surfaces depends on more than 100 additive manufacturing (AM) process parameters. To facilitate using metal AM parts in engineering applications, it is important to understand the traction relationship as a function of the surface topography of the as-built surfaces. Figure 6 shows (a) a picture

of the specimen (ASTM E466-15), manufactured using a 3D Systems ProX DMP 320 L-PBF machine with recycled powder (mean diameter 39.98 μm), bulk laser power 220 W, contour laser power 115 W, hatch spacing 100 μm , layer thickness 30 μm , bulk scan speed 1180 mm/s, and contour scan speed 625 mm/s. The details of the manufacturing process are specified in [42, 43]. Figure 6b shows a confocal microscopy image (Olympus LEXT OLS5000) of the as-built surface topography, using a 20 \times objective lens, and a 6 mm \times 6 mm area, after post-processing using a Gaussian filter according to ISO4287 [7].

Figure 7a shows the probability density function $\Phi(h/h_{rms})$ of the non-dimensional surface height (solid line) compared to the standard normal distribution $\mathcal{N}(0, 1)$ (dotted line). The distribution shows a kurtosis of 3.613 and a skewness of 0.4242, i.e., it is close to a Gaussian distribution. Thus, we consider h/h_{rms} to follow a Gaussian distribution. We point out that most engineering surfaces display a non-Gaussian distribution of surface heights h/h_{rms} because they show a preferential manufacturing direction. Furthermore, Fig. 7b shows the PSD as a function of the non-dimensional wavenumber k/k_1 and for $k_r/k_1 = 1$ (solid line). We also

Fig. 8 The non-dimensional mean pressure $\bar{p}/E^*k_1h_{rms}$ versus the non-dimensional mean gap \bar{g}/h_{rms} for the as-built Inconel 718 surface with $H = 0.6270$ and $k_r/k_1 = 1$, calculated from the best-fit regressing equations (7)–(8)



show the linear best-fit of the PSD (dashed line), and we determine that $H \approx 0.6270$ with $k_r/k_1 = 1$. Thus, using these parameters, we determine the traction relationship from the best-fit regression equations (7)–(8).

Figure 8 shows the traction relationship for the as-built Inconel 718 surface with $H = 0.6270$, $k_r/k_1 = 1$, $k_1 = 2\pi/6 \text{ mm}^{-1}$ and $h_{\text{rms}} = 17.7 \mu\text{m}$, in contact with a rigid flat. We also indicate the region in which we approximate the traction relationship with the exponential function ($0.5 \leq g/h_{\text{rms}} \leq 1.5$) and the complementary error function ($1.5 \leq g/h_{\text{rms}} \leq 6.0$). Parameter A of the complementary error function best-fit is 0.3 times parameters A of the exponential function best-fit to satisfy the continuity condition at $g/h_{\text{rms}} = 1.5$, and parameters B is the constant 0.478.

5 Conclusion

- (1) We derived best-fit regression equations that approximate the non-dimensional traction relationship expressed by Eq. (2), to render this model practically accessible for use in engineering applications. We showed that the traction relationship between random rough surfaces is best approximated by an exponential function [Eq. (6)] when ($0.5 \leq \bar{g}/h_{\text{rms}} \leq 1.5$) and by a complementary error function [Eq. (5)] when ($1.5 \leq \bar{g}/h_{\text{rms}} \leq 6.0$).
- (2) In contrast to previous publications [27, 28, 40] that consider a rough surface within the fractal range, i.e., $k_r/k_1 = 1$, we included the effect of roll-off wavenumber, and derived best-fit regression parameters as a function of the random roughness PSD shape factors H and k_r/k_1 . We confirmed that the best-fit regression equations follow an exponential function and the complementary error function independent of the roll-off wavenumber. However, the regression coefficient A showed a linear relationship with k_r/k_1 , whereas the regression coefficient B remained constant at $\sqrt{2}$ and 0.48 for the complementary error function and the exponential function, respectively. Therefore, one may use linear extrapolation to obtain the traction relationship for a surface with a larger k_r/k_1 than the one we presented. Furthermore, decreasing H increases the contribution of the fine-scale roughness and, thus, it changes the regression coefficient A to increase \bar{p} .
- (3) According to dimensional analysis, \bar{p} is determined by three surface topography parameters H , k_r/k_1 , and $h_{\text{rms}}k_1$ for different values of \bar{g}/h_{rms} . To illustrate the use of the best-fit regression equations derived in this paper, we obtained the surface topography parameters from an as-built Inconel 718 surface manufactured using L-PBF, and we derived the traction relationship.

Additionally, we observed that the as-built surface exhibits fractal properties with $0.6 < H < 0.7$.

Funding This work was supported by the Department of Defense, Office of Local Defense Community Cooperation, under Award No. ST1605-21-04.

Data Availability Source data available by request.

Code Availability We used custom code developed by our lab.

Declarations

Conflict of interest The authors declare no conflicts of interest or competing interests.

References

1. Bowden, F.P., Tabor, D.: The Friction and Lubrication of Solids, vol. 1. Oxford University Press, Oxford (2001)
2. Barber, J.R.: Bounds on the electrical resistance between contacting elastic rough bodies. Proc. R. Soc. Lond. A **459**(2029), 53–66 (2003)
3. Lorenz, B., Persson, B.N.J.: Leak rate of seals: comparison of theory with experiment. Europhys. Lett. **86**(4), 44006 (2009)
4. Dapp, W.B., Lücke, A., Persson, B.N.J., Müser, M.H.: Self-affine elastic contacts: percolation and leakage. Phys. Rev. Lett. **108**(24), 244301 (2012)
5. Akarapu, S., Sharp, T., Robbins, M.O.: Stiffness of contacts between rough surfaces. Phys. Rev. Lett. **106**(20), 204301 (2011)
6. Quinn, D.D., Segalman, J.: Using series-series Iwan-type models for the understanding of joint dynamics. J. Appl. Mech. **72**(5), 666–673 (2005)
7. ISO 4287: Geometrical Product Specifications (GPS)-Surface Texture: Profile Method-Terms. Definitions and Surface Texture Parameters. ISO (2019)
8. Pastewka, L., Robbins, M.O.: Contact between rough surfaces and a criterion for macroscopic adhesion. Proc. Natl Acad. Sci. USA **111**(9), 3298–3303 (2014)
9. Müser, M.H., Dapp, W.B., Bugnicourt, R., Sainsot, P., Lesaffre, N., Lubrecht, T.A., Persson, B.N.J., Harris, K., Bennett, A., Schulze, K., et al.: Meeting the contact-mechanics challenge. Tribol. Lett. **65**(4), 1–18 (2017)
10. Greenwood, J.A., Williamson, J.P.: Contact of nominally flat surfaces. Proc. R. Soc. Lond. A **295**(1442), 300–319 (1966)
11. Bush, A.W., Gibson, R.D., Thomas, T.R.: The elastic contact of a rough surface. Wear **35**(1), 87–111 (1975)
12. Nayak, P.R.: Random process model of rough surfaces. ASME J. Tribol. **93**(3), 398–407 (1971)
13. Greenwood, J.A., Wu, J.J.: Surface roughness and contact: an apology. Meccanica **36**(6), 617–630 (2001)
14. Mandelbrot, B.B., Passoja, D.E., Paullay, A.J.: Fractal character of fracture surfaces of metals. Nature **308**(5961), 721–722 (1984)
15. Persson, B.N.J.: On the fractal dimension of rough surfaces. Tribol. Lett. **54**(1), 99–106 (2014)
16. Persson, B.N.J., Albohr, O., Tartaglino, U., Volokitin, A., Tosatti, E.: On the nature of surface roughness with application to contact

- mechanics, sealing, rubber friction and adhesion. *J. Phys. Condens. Matter* **17**(1), 1 (2004)
17. Ciavarella, M., Demelio, G., Barber, J.R., Jang, Y.H.: Linear elastic contact of the Weierstrass profile. *Proc. R. Soc. Lond. A* **456**(1994), 387–405 (2000)
 18. Persson, B.N.J.: Theory of rubber friction and contact mechanics. *J. Chem. Phys.* **115**(8), 3840–3861 (2001)
 19. Wang, A., Müser, M.H.: Gauging Persson theory on adhesion. *Tribol. Lett.* **65**(3), 1–10 (2017)
 20. Müser, M.H.: Response to a comment on meeting the contact-(mechanics) challenge. *Tribol. Lett.* **66**(1), 1–6 (2018)
 21. Joe, J., Thouless, M.D., Barber, J.R.: Effect of roughness on the adhesive tractions between contacting bodies. *J. Mech. Phys. Solids* **118**, 365–373 (2018)
 22. Joe, J.: Traction between rough surfaces. PhD Thesis (2021)
 23. Yang, C., Persson, B.N.J.: Molecular dynamics study of contact mechanics: contact area and interfacial separation from small to full contact. *Phys. Rev. Lett.* **100**(2), 024303 (2008)
 24. Johnson, K.L.: *Contact Mechanics*. Cambridge University Press, Cambridge (1987)
 25. Campaná, C., Müser, M.H.: Practical Green's function approach to the simulation of elastic semi-infinite solids. *Phys. Rev. B* **74**(7), 075420 (2006)
 26. Pastewka, L., Prodanov, N., Lorenz, B., Müser, M.H., Robbins, M.O., Persson, B.N.J.: Finite-size scaling in the interfacial stiffness of rough elastic contacts. *Phys. Rev. E* **87**(6), 062809 (2013)
 27. Persson, B.N.J.: Relation between interfacial separation and load: a general theory of contact mechanics. *Phys. Rev. Lett.* **99**(12), 125502 (2007)
 28. Pohrt, R., Popov, V.L.: Normal contact stiffness of elastic solids with fractal rough surfaces. *Phys. Rev. Lett.* **108**(10), 104301 (2012)
 29. Violano, G., Papangelo, A., Ciavarella, M.: Stickiness of randomly rough surfaces with high fractal dimension: is there a fractal limit? *Tribol. Int.* **159**, 106971 (2021)
 30. Yastrebov, V.A., Anciaux, G., Molinari, J.: On the accurate computation of the true contact-area in mechanical contact of random rough surfaces. *Tribol. Int.* **114**, 161–171 (2017)
 31. Monti, J.M., Pastewka, L., Robbins, M.O.: Fractal geometry of contacting patches in rough elastic contacts. *J. Mech. Phys.* **160**, 104797 (2022)
 32. Dieterich, J.H., Kilgore, B.D.: Direct observation of frictional contacts: new insights for state-dependent properties. *Pure Appl. Geophys.* **143**(1), 283–302 (1994)
 33. Dieterich, J.H., Kilgore, B.D.: Imaging surface contacts: power law contact distributions and contact stresses in quartz, calcite, glass and acrylic plastic. *Tectonophysics* **256**(1–4), 219–239 (1996)
 34. Majumdar, A., Bhushan, B.: Role of fractal geometry in roughness characterization and contact mechanics of surfaces. *ASME J. Tribol.* **112**(2), 205–216 (1990)
 35. Campaná, C., Müser, M. H.: Contact mechanics of real vs. randomly rough surfaces: a Green's function molecular dynamics study. *Europhys. Lett.* **77**(3), 38005 (2007)
 36. Hyun, S., Pei, L., Molinari, J., Robbins, M. O.: Finite-element analysis of contact between elastic self-affine surfaces. *Phys. Rev. E* **70**(2), 026117 (2004)
 37. Berthoud, P., Baumberger, T.: Shear stiffness of a solid–solid multicontact interface. *Proc. R. Soc. Lond. A* **454**(1974), 1615–1634 (1998)
 38. Barber, J.R.: *Contact Mechanics*. Springer, Berlin (2018)
 39. Buzio, R., Boragno, C., Biscarini, F., De Mongeot, F.B., Valbusa, U.: The contact mechanics of fractal surfaces. *Nat. Mater.* **2**(4), 233–236 (2003)
 40. Papangelo, A., Hoffmann, N., Ciavarella, M.: Load–separation curves for the contact of self-affine rough surfaces. *Sci. Rep.* **7**(1), 1–7 (2017)
 41. Blakey-Milner, B., Gradl, P., Snedden, G., Brooks, M., Pitot, J., Lopez, E., Leary, M., Berto, F., du Plessis, A.: Metal additive manufacturing in aerospace: a review. *Mater. Des.* **209**, 110008 (2021)
 42. Watring, D.S., Carter, K.C., Crouse, D., Raeymaekers, B., Spear, A.D.: Mechanisms driving high-cycle fatigue life of as-built Inconel 718 processed by laser powder bed fusion. *Mater. Sci. Eng. A* **761**, 137993 (2019)
 43. Detwiler, S., Watring, D., Spear, A., Raeymaekers, B.: Relating the surface topography of as-built Inconel 718 surfaces to laser powder bed fusion process parameters using multivariate regression analysis. *Precis. Eng.* **74**, 303–315 (2022)

Publisher's Note Springer Nature remains neutral with regard to jurisdictional claims in published maps and institutional affiliations.